Review Vol. 16, No. 2 / 1 Feb 2025 / Biomedical Optics Express 578
Biomedical Optics EXPRESS

Robotics and optical coherence tomography: current works and future perspectives [Invited]

GUANGSHEN MA,[1] MORGAN MCCLOUD,[2] YUAN TIAN,[2] AMIT NARAWANE,[2] HARVEY SHI,[2] ROBERT TROUT,[2] RYAN P. MCNABB,[3] ANTHONY N. KUO,[2,3] AND MARK DRAELOS[1,4]

[1]*Department of Robotics, University of Michigan, Ann Arbor, MI 48105, USA*
[2]*Department of Biomedical Engineering, Duke University, Durham, NC 27705, USA*
[3]*Department of Ophthalmology, Duke University Medical Center, Durham, NC 27705, USA*
[4]*Department of Ophthalmology and Visual Sciences, University of Michigan Medical School, Ann Arbor, MI 48105, USA*

Abstract: Optical coherence tomography (OCT) is an interferometric technique for micron-level imaging in biological and non-biological contexts. As a non-invasive, non-ionizing, and video-rate imaging modality, OCT is widely used in biomedical and clinical applications, especially ophthalmology, where it functions in many roles, including tissue mapping, disease diagnosis, and intrasurgical visualization. In recent years, the rapid growth of medical robotics has led to new applications for OCT, primarily for 3D free-space scanning, volumetric perception, and novel optical designs for specialized medical applications. This review paper surveys these recent developments at the intersection of OCT and robotics and organizes them by degree of integration and application, with a focus on biomedical and clinical topics. We conclude with perspectives on how these recent innovations may lead to further advances in imaging and medical technology.

1. Introduction

OCT is a well-established non-invasive, high-resolution volumetric optical imaging technique that enables near real-time visualization of biological tissue microstructures [1,2]. Since the first OCT cross-sectional *in vivo* imaging of the eye [3,4], OCT research has yielded improvements in data acquisition rate and quality, image interpretation, and diagnostic capability in numerous disease states [5–8]. These capabilities have led to growing interest in OCT as a high-resolution vision or perception system for robots, especially in clinical or biomedical domains. For example, recent combinations of robotics and OCT include large-area tissue scanning [9,10], object tracking [11], or image-guided robotic surgery [12–14]. In space-constrained environments, such as robotic endoscopic surgery [15,16], researchers have co-developed novel optical designs and robot control algorithms to enable new or less invasive procedures [15,17]. These works and others have produced efficient algorithms for guiding robotic OCT systems, novel hardware architectures or integrations, and unique optical designs for next-generation instruments.

Conventional robot 3D perception systems rely on camera-based technologies, including stereo cameras [18], microscope cameras [19], and structured light illumination [20], which can produce "2.5D" topographic data (depth of a single surface) instead of 3D volumetric data. For medical robots, diagnostic and intraoperative tomographic imaging (e.g. magnetic resonance imaging [MRI] and computed tomography [CT] [21]) have a role for real-time imaging and assisting in surgical navigation but add considerable complexity and bulk. In contrast to these techniques, OCT exhibits fast, high-fidelity volumetric scanning in a compact form factor that facilitates direct system integration [22,23]. Working synergistically, robotic OCT systems can further expand the workspace of traditional tabletop OCT systems and allow for multiple views and positions of dynamic samples. These advantages of OCT render it suitable for integration into existing medical robotics systems to enable a broad range of applications, including diagnostics, robotic

#547943 https://doi.org/10.1364/BOE.547943
Journal © 2025 Received 14 Nov 2024; revised 29 Dec 2024; accepted 1 Jan 2025; published 16 Jan 2025

Biomedical Optics EXPRESS

surgery, tissue manipulation, and exploration of fundamental research problems in micro-level biological systems [24–26]. Moreover, the rate of such integrations is accelerating, as evidenced by many recent publications on this topic [22,23,27].

In this paper, we therefore review recent advances and innovations in robotic OCT. Previous reviews have focused on the fundamentals of OCT [28], OCT for intraoperative visualization with applications in open surgery [23], OCT applications in oncology [22], and ophthalmology applications for the diagnosis of retinal diseases [29,30]. Instead, we review the novel ways in which researchers have blended robotics and OCT. As the majority of robot-OCT systems are targeted for biomedical applications, we focus our review on the development of medical robots and the associated applications in translational medicine and clinics. We first briefly present the core background for OCT and robotics separately and then consider existing robotic OCT systems organized by their degree of integration. We next discuss enabling technologies that facilitate OCT use in robotics and conclude with future directions for robotic OCT research.

2. Background

2.1. Optical coherence tomography

Optical coherence tomography (OCT) is a non-invasive volumetric imaging technique that applies low coherence interferometry to light from multiple reflectors to produce depth-resolved images beneath the surface of objects [31]. This capability is particularly valuable in biomedical applications since OCT can penetrate biological tissue and produce images from within the tissue surface. Conventional OCT utilizes an interferometer (typically either Michelson or Mach-Zehnder topology) with a coherent source, reference arm, sample arm, and detector. For a point-scan OCT sample arm, scanning optics move the focused beam laterally across the tissue surface [32]. At each lateral beam position, the light from the sample interferes with the light from the reference arm to produce a one-dimensional signal that represents the positions of the reflective tissue layers in axial depth ("A-scan"). As the beam is scanned across the entire sample, a series of A-scans are collected to formulate cross-sectional ("B-scans") and 3D volumetric images ("C-scans"). By this means, OCT provides non-invasive, high-resolution images at high speed, producing sample or tissue measurements suitable for use with robot systems. For robotics applications that require a high signal-to-noise ratio and high measurement speed (A-scan rate of 25 kHz to beyond 1 MHz), Fourier-domain OCT (FD-OCT) and swept-source OCT (SS-OCT) are the most suitable [33,34]. In summary, the effective implementation of the robotic OCT system relies on the overall design of the OCT engine and the configuration of the robot system.

The OCT scanner's field of view (FOV) determines the area over which the beam can be scanned and is chosen for the particular application, such as large-area retinal imaging for surgical planning or small-area imaging for precise manipulation of robotic instruments [35–38]. Common OCT systems are designed with limited field of view in the lateral direction (e.g., 10 to 20 millimeters) and the axial direction (e.g., 2 to 5 millimeters) depending on the specialized design of the OCT engine [23,38]. Thus, a tabletop OCT can capture a small tissue object with high-resolution cross-sectional images or 3D volume within the scanning regions. For example, the cornea would normally have a diameter of approximately 11.5 to 11.7 mm [39] and a thickness of approximately 0.5 mm in the central region [40]. The diameters of typical tools in ophthalmic microsurgery can range from 0.26 to 0.41 mm depending on surgical applications and types of microsurgery [41,42]. Small targets such as these can fit within a fixed OCT scanning region; however, larger tissues, such as the kidney [10] and the human arm [43], pose challenges with a small field of view. This motivates the development of robotic OCT systems and advanced algorithms to expand scanning capability and register multiple OCT measurements for high-fidelity image reconstruction.

Biomedical Optics EXPRESS

2.2. Robotics

A robot system consists of the robot's mechanical assembly (e.g., robot arm) for positioning its end-effector, the control units for its joints, and a mathematical description of how the robot moves in 3D space (kinematics) [44,45]. When connected to the robot's controller, sensors allow the robot to detect objects within its environments and form the basis of a perception system. In addition, the sensors can provide real-time imaging feedback to update the control output and planning strategy. Using OCT to monitor the dynamics of tissue samples enables the development of high-level control and motion planning methods that can be deployed to robotic systems, which can be used to achieve dexterous manipulation of surgical tools or execute complex actions commanded by surgeons through remote control [45]. With fast data acquisition and sufficient sub-surface depth information, OCT can be combined with medical robotics for the development of advanced methods that can be used in the evaluation of previously inaccessible tissues, automatic tool detection using machine learning models and robotic surgery [46].

For common robotic OCT configurations, OCT (either the sample arm or entire system) can be mounted to the robot end-effector to formulate a unified system for free-space scanning [43,47–49] or serve as a tabletop sensor module to work with robot-controlled instruments [50–53]. For the former configuration, the hardware setup for the OCT module can be independently optimized to achieve improved imaging performance without affecting the sensing or robot systems. The design of the integrated OCT system should account for the robot's payload limit and repeatability and for mechanical mounting constraints to optimize the robot workspace [37]. Conversely, for the latter configuration, OCT serves as a sensing system to evaluate tissue during the robot-controlled tool-tissue interaction. This physical interaction is a function of the design of surgical tools, including the needle or probe [52,54,55], tissue properties, and the robot planning and control algorithms used with OCT B-scan and C-scan imaging feedback [14,56]. Additionally, there are unique cases where non-integrated OCT systems cannot be directly applied to the medical procedures such as scanning of internal organs under constrained environments [25,26]. Given these special requirements, system development requires novel optical designs as well as careful consideration of robot systems and OCT sensors for integration. Depending upon the diversity of medical applications, robotic OCT systems have specialized designs of software, hardware, and optics to jointly optimize the OCT scanning performance.

3. Integration approaches

Robotic OCT systems can be classified mainly as four different configurations based on geometric relations between robots and sensors: robot-adjacent OCT, robot-mounted OCT, robot-guided OCT sensing tools, and endoscopic OCT. The robot-adjacent OCT and robot-mounted OCT approaches give rise to "OCT-guided robot systems" that differ in the physical location of the sensor relative to the robot end-effector. For special medical needs in endoscopy and eye surgery, robot-guided OCT sensing tools and endoscopic OCT give rise to "Robot-guided OCT systems" where the robot functions to deliver novel optics to the target location in specialized medical scenarios. In this section, we discuss the system designs and medical applications associated with these four robotic-OCT configurations, as shown in Fig. 1.

3.1. Robot-adjacent OCT

A robot-adjacent OCT system is comprised of a tabletop OCT system to provide imaging feedback and a robot system to execute high-level control algorithms for robot manipulations [50,52,59,60]. In common setups, the OCT sensor is at a fixed location viewing the objects and the robot controls a medical instrument for accurate and dexterous manipulation. In this section, we introduce different robot-instrument combinations that have been widely used in robot-adjacent OCT systems and discuss their applications in robotic surgery and surgical guidance.

Biomedical Optics EXPRESS

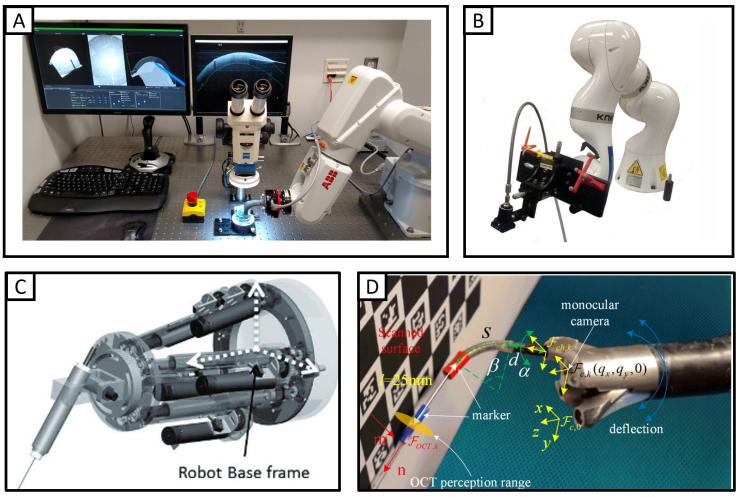

Fig. 1. Overview of the four Robot-OCT configurations. (A) Robot-adjacent OCT setup with a 1060 nm SS-OCT sample arm in the microscope and an adjacent robot-controlled needle system with a 6-axis robot arm. Adapted from [14]. (B) Seven-axis robot manipulator with an OCT-guided optical system mounted to its end-effector. Adapted from [57]. (C) An OCT-forceps probe integrated with and controlled by a 6-DOF parallel robot system. Adapted from [58]. (D) An endoscopic robot with an OCT probe for optimization-based visual servoing control. Adapted from [15].

3.1.1. OCT image feedback for robotic tool control

Robot-adjacent OCT configurations normally consist of a robot manipulator holding a medical instrument guided by a tabletop OCT system. Common types of medical tools are needles [12,14,51,53], probes [55,61–63], and specialized instruments, such as laser scalpels [64]. In particular, needle tools have been widely applied in OCT-guided robotic ophthalmic microsurgery [51–53,56,65]. In these studies, high-level controllers are used to guide the needles toward the surgical target using segmentation results from B-scan or C-scan data [50,52,66]. Based on the micrometer-scale accuracy and the fast data acquisition of the OCT sensor, OCT-guided needle insertion systems have been developed primarily for eye surgery, including deep anterior lamellar keratoplasty (DALK) [12,14], retinal vein cannulation [67–69], and subretinal injections [51,70]. In the case of probes, which can apply external force to tissues, previous work has focused on the development of computer vision methods and machine learning models to estimate applied force by using swept-source OCT for volumetric data collection [55,62,63].

Tabletop robotic OCT systems have also been applied to provide imaging feedback to guide instrument movements in various types of robot systems. For example, Zhu et al. proposed a laser-based surgical system that can provide global structural information for murine tumor scanning [64]. In this study, laser-based autofluorescence spectroscopy and an OCT sensor were integrated with a XY-translational robot stage for intraoperative diagnosis. Giudice et al. proposed another work for the development of an OCT-guided visual servo control platform with a continuum robot, where the OCT was fixed facing the continuum robot to provide imaging feedback [71]. Baran et al. reported preliminary results on the use of a fixed OCT probe for the position control of a concentric tube robot [72]. Moreover, a tabletop OCT system can also be used to estimate tissue motion through a 6 degree-of-freedom (DOF) robot controlled surgical field where the OCT scanner can collect imaging data while the tissue object is moving [60]. With a fixed OCT setup, the surgical site can be manipulated by a 6 DOF parallel robot while the tissue is moved to arbitrary positions scanned by the OCT sensor [73].

Biomedical Optics EXPRESS

A summary of different surgical tools with the adjacent OCT configuration is shown in Fig. 2. This figure introduces the existing works with different instrument-OCT combinations in the robot-adjacent OCT systems category.

3.1.2. Solving robotic tool-tissue perception problems with OCT

Tool-tissue interaction encompasses many research problems associated with robot-adjacent OCT systems that aim to study how tissue structure changes during robotic manipulations. OCT has demonstrated excellent capability in measuring spatial relationships between the attached tool and tissue based on its functions of visualizing micrometer-scale tissue structures and capturing volumetric imaging feedback to solve perception problems. In this section, we review applications related to tool-tissue interaction with a focus on computer vision algorithms and force sensing problems for OCT-based perception.

In the context of robotics, OCT sensors function as 3D perception systems to provide micrometer resolution volumetric scanning to study or monitor tissue-tool interactions. Specific perception problems that benefit from OCT image guidance include tool tracking, localization, and segmentation. For example, Keller et al. proposed a surgical tool tracking algorithm and a corneal boundary segmentation algorithm for intraoperative OCT data [75]. The tool tracking algorithm is based on the connected component algorithm and the principal component analysis (PCA) to estimate the position of the needle tip. The corneal segmentation algorithms are based on OCT B-scan gradients and graph search algorithms. Weiss et al. developed a fast 5-DOF needle tracking system for intraoperative cross-sectional OCT images using an application-specific Kalman filter [76]. In addition to using conventional image processing methods, deep learning models, such as U-net architectures, have shown great potential in OCT for tool tracking and tissue segmentation [42,65,77,78]. To provide fast inferences and real-time performance for needle tip detection, Park et al. utilized a convolutional neural network to segment the needle and cornea in OCT volumes [65]. Xu et al. implemented a U-net deep learning framework to segment the tool and the retina in images from a spiral scan pattern for fast needle tracking [79]. In addition, research has been conducted on the estimation of tool-to-layer distance by using intraoperative 4D OCT and a convolutional neural network [80]. In summary, deep learning algorithms have enabled significant advancements in OCT-guided medical imaging analysis including segmentation, detection, and classification.

In addition to tool manipulation inside tissue samples, probe-tissue interaction is a recently explored problem in the robot-OCT domain. Previous research has explored solutions for robust force control to ensure safety and estimate forces using OCT B-scan or C-scan images [53,55,61,81]. In these studies, the OCT data was directly supplied to feature extractors and encoders for force value predictions, and some research works have switched to the use of deep learning methods for force classification using the OCT data [62,63].

3.1.3. OCT-guided robotic surgery

With an adjacent OCT setup, robotic surgery requires intelligent control and advanced perception algorithms to accomplish the sub-tasks of tool tracking, segmentation, and localization during robotic soft-tissue manipulation procedures. Although OCT can provide high-resolution images during surgery, motion tracking and surgical tool manipulation remain challenging problems due to OCT's small field of view (FOV) and the surgeon's hand tremor, where the development of advanced robot control algorithms and visualization methods is needed. This section reviews the research studies of OCT-guided robot controllers and planners, as well as system development strategies for robotic surgery.

In applications of ophthalmic surgery, the robotic-adjacent OCT is a common design and features in multiple applications, including subretinal needle injections [51,70], DALK [14,65,66], automated suturing [82], and automated retinal vein cannulation [69]. For anterior surgery,

Biomedical Optics EXPRESS

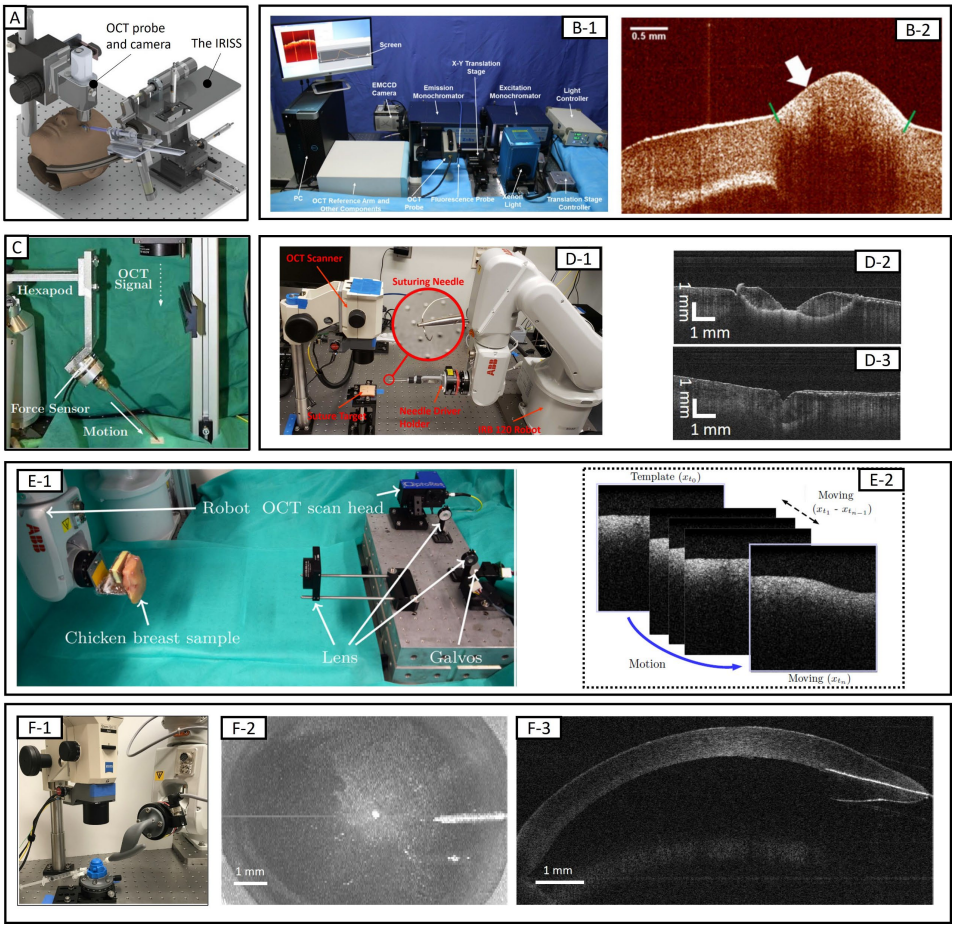

Fig. 2. Overview of robot-adjacent configurations for robot-guided medical applications. (A) A tabletop OCT system with the intraocular robotic interventional surgical system (IRISS) in cataract surgery. Adapted from [74]. The objective lens exhibits a focal length of 54 mm and a 10 × 10 mm field of view. (B) B-1 shows the dual-modality system with a tabletop OCT for robotic laser surgery with applications for tumor resection in neurosurgery. The tumor was imaged in a 5 mm × 5 mm region of interest with an imaging depth of approximately 2 mm. B-2 depicts an OCT image of the tumor upper surface. B-1 and B-2 are adapted from [64]. (C) Tabletop OCT system to collect data from a deformable phantom for a surgical pushing task performed by a Hexapod robot. Adapted from [62]. The OCT volume covers a field of view of 3 mm × 3 mm × 3.5 mm. (D) D-1 shows the tabletop OCT system platform for robot-controlled automated suturing. D-2 and D-3 depict OCT B-scan images before and after the wound edge closure from OCT-guided suturing. Adapted from [50]. (E) E-1 shows the tabletop OCT system to estimate tissue motion produced by a 6-DOF robot arm (OCT volume with a field of view of 5 mm × 5 mm × 3.5 mm). E-2 depicts the sequence of OCT images for motion estimation. E-1 and E-2 are adapted from [60]. (F) F-1 shows a 3D printed handle holding the surgical needle to an artificial anterior chamber based on a robot-OCT system with an IRB 120 industrial robot arm manipulator (ABB, Zurich, Switzerland). F-2 depicts an en face OCT view of a needle in cornea. F-3 describes the OCT B-scan image of the cross-sectional view along the needle's axis. (The scalebar is adjusted for F-2 and F-3. F-1, F-2 and F-3 are adapted from [56]).

Biomedical Optics EXPRESS

Draelos et al. showed a cooperative mode OCT-guided robot needle insertion system for partial-thickness cornea transplant surgery [83]. In this scheme, the surgeon holds the robot end effector and guides the arm to insert the needle into the cornea while the needle insertion depth is reported in real-time. To enable real-time and fast tracking of surgical tools towards targets, Zhou et al. proposed a marker-free robot-OCT hand-eye calibration technique for robot-assisted vitreoretinal surgery [42,84]. They installed the needle on the end-effector of a custom robot arm and acquired OCT volumes to identify the needle tip position. A hand-eye calibration algorithm was implemented to optimize the position between the needle tip and the OCT with micron-level errors. Their proposed calibration method was also extended to 6-DOF using the iterative closest point (ICP) algorithm and was capable of achieving micro-level calibration errors [85]. Instead of a serial robot arm, Charreyron et al. used a magnetically-driven continuum robot to perform OCT-guided sub-retinal injections in *ex vivo* porcine eyes [86]. Some research topics have also focused on the development of advanced algorithms for fully-automated surgery. Shin et al. demonstrated an automatic corneal suturing robot by designing a vacuum-based corneal holding device [82]. They verified the final suturing path through OCT B-scans. In addition to the straight needle insertion, Tian et al. proposed automatic curved suturing needle insertion under OCT guidance [50]. Using the iterative closest point (ICP) algorithm, the system calibrated the robot-needle frame and the robot-OCT frame at the same time. After identifying the shape and depth of the wound, a suturing path was generated to guide the needle insertion procedure.

With advances in machine learning for robot control, researchers have developed reinforcement learning frameworks for automated eye surgery [56]. For OCT-guided applications, the data-driven model can interpret OCT volumes to produce appropriate robot needle trajectories in a fully-automated manner through learning from demonstration [56]. Additionally, Edwards et al. proposed a data-driven method to use an auto-regressive model to update tool positions based on the tracked surgical tool and segmented biological tissue boundary [66]. This method aimed to leverage the tool tracking from B-scan images to design controllers for eye surgery. A system with a data-driven autoregressive dynamics model and a model predictive controller has been successfully implemented to improve needle placement accuracy.

OCT can also be used as an advanced visualization tool to assist surgeons in surgical teleoperation. For example, Edwards et al. conducted the first-in-human study for remote control of intraocular robotic surgery and used intraoperative OCT to visualize the surgical field [87]. This work demonstrated the superior capability of OCT for robotic surgery and intraoperative visualization. However, the high resolution and small scan region of OCT-based volumetric reconstruction can pose challenges for surgeons to guide their maneuvers using real-time OCT data. Virtual reality (VR) and augmented reality (AR) offer an alternative display scheme that can improve surgeons' user experience [88]. VR and AR systems can be integrated with robot systems to help surgeons reliably perform surgical maneuvers with teleoperated systems [89,90]. Additionally, Tang et al. proposed a microscope-integrated OCT system for AR applications with the vision of helping surgeons align 3D OCT data with 2D data by using a novel registration method and robot arm manipulation [91].

3.2. Robot-mounted OCT

A second robotic OCT configuration involves mounting an OCT sensor to the end-effector of the robot system. The OCT sensor can be controlled by the robot to move to arbitrary positions and orientations in 3D space, which allows for the extended scanning capabilities of multi-view and large-area scanning [35,47,89]. This configuration has been widely used with 6-DOF and 7-DOF robot systems with integrated OCT modules attached to the end-effector [43,48,49,92,93], as well as with the 5-DOF robot system [94]. In this section, we review robot-mounted OCT systems with different combinations of OCT sensor designs and robot mechanisms.

Biomedical Optics EXPRESS

3.2.1. System and hardware configurations

Robot-mounted OCT is normally formulated with an integrated OCT sensor and a robot manipulator with arbitrary degrees of freedom (Fig. 3). A common example is the robot arm manipulator that has been widely used with built-in OCT scanners to achieve open-space scanning. Draelos and Ortiz et al. have proposed a generalized platform that uses a robotic OCT system for free-space arbitrary-viewpoint scanning of the cornea and retina [37,95]. This system incorporated complementary sensors including RGB-D cameras for face tracking and pupil cameras for eye position and gaze tracking. For 1.2 kg anterior and 2.3 kg retinal scan heads, the commercial UR3 robot arm (Universal Robots) had appropriate 3 kg payload and 0.1 mm repeatability. Furthermore, they demonstrated multiple *in vivo* applications of eye imaging [47] and eye tracking under subject motion [96,97]. Using a similar robot end-effector configuration, He et al. proposed a 6-DOF robotic OCT system for large field of view scanning for continuous scanning of monolithic storage devices by using a robot arm with a payload of 3 kg [35]. This system offers an adjustable field of view OCT scanning capability with a lateral resolution of about 7 μm and an axial resolution of about 4 μm. Their study also demonstrated high-fidelity volumetric scanning of storage devices for the identification of abnormal electrical connections, device inspection, and microsurgery with laser ablations with ± 10 μm precision. Furthermore, Huang et al. proposed another solution to solve the limited field of view problem by using a 7-DOF robot-OCT system based on a stop-and-scan strategy [38]. The single 3D OCT FOV is reported as 4.1 mm × 4.1 mm × 3.6 mm for volumetric measurement and the 7-DOF robot arm system can achieve a positioning accuracy of approximately 0.1 mm. Li et al. developed a sensor fusion system using the structured 3D light system to create a pre-defined trajectory for OCT-guided large-region scanning [20]. Lotz et al. proposed a calibration-free robot-OCT system for large-area scanning by using a custom-built swept-source OCT system [43]. This system does not rely on complete system calibration and registration between the OCT and other machine vision systems. Moreover, robot-mounted OCT systems also include those with fiber-based OCT sensors. For example, Jivraj et al. developed an integrated OCT system for dynamic refocusing of the surgical laser by using a 7-DOF robot arm [57].

In summary, these systems focus mainly on combinations of integrated OCT systems, commercialized robot manipulators, and complementary sensors to provide sufficient scanning capabilities for large-area free-space scanning. Engineering solutions, including cable management to minimize potential collisions between systems and target tissue [37,43], sensor suite designs for the robot arm end-effector based on the accuracy and precision requirements, and fast OCT data acquisitions for efficient large-area scanning, are also proposed in the literature. These innovations and technologies in robot-OCT systems can motivate the development of advanced robot control and planning algorithms for the improvement of scanning efficiency.

3.2.2. Application for large-area scanning

Although OCT is effective for micron-resolution imaging of small regions of interest, there are many clinical scenarios in which a much larger field of view is needed. To address this problem, multiple groups have mounted OCT systems on robotic arms to enable large area field of view imaging by moving the robot and mosaicking the resulting images together [20,38,43,48]. This enables OCT imaging of targets that occupy a large range in space, including organ, limb, and even whole-body imaging. Robotic platforms for OCT scanners have demonstrated promise in this area, enabling the repositioning of the imaging head to tile a space far larger than its optical field of view and depth falloff. In this way, an image of far greater dimensions can be reconstructed using motion data sensed from the robotic component [20,38]. These technologies have great potential in fields where high resolution depth sensitive imaging is required for diagnostics but must be performed over a very large surface area, including clinical scenarios within neurology [49,98,99], ophthalmology [100,101], dermatology [43], and organ transplant monitoring [10].

Biomedical Optics EXPRESS

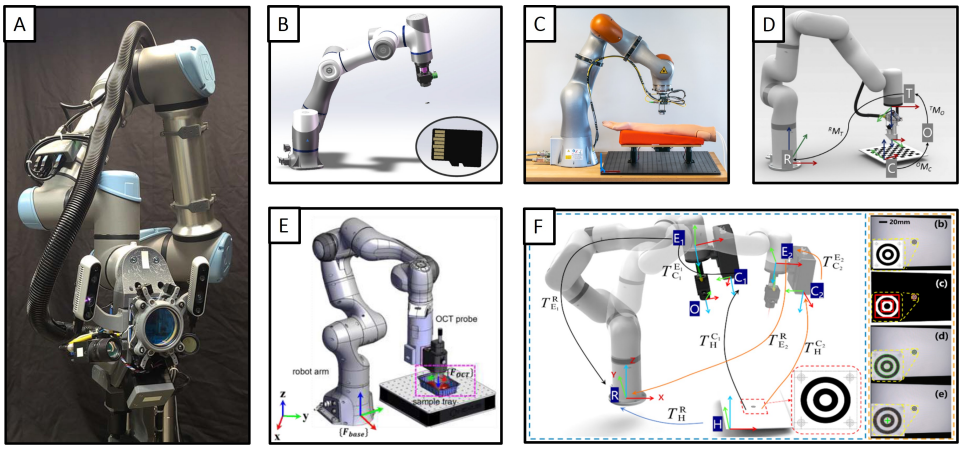

Fig. 3. Overview of robot-mounted OCT systems with OCT scanner attached to 6-DOF or 7-DOF robot manipulator. (A) An integrated galvanometer-based OCT system attached to a 6-DOF robot arm with complementary sensors for face and pupil tracking. Adapted from [37]. (B) A 6-DOF robotic OCT system for inspection of monolithic storage devices and laser-based microsurgery tasks. Adapted from [35]. (C) A large-area robotically assisted optical coherence tomography (LARA-OCT) system with a 7-DOF robot arm and a 3.3MHz swept-source OCT sensor. Adapted from [43]. (D) Large field of view scanning with robot-mounted OCT system. Adapted from [38]. (E) An integrated OCT system with 6-DOF manipulator for large-area kidney scanning. Adapted from [10]. (F) A 6-DOF robot system equipped with a portable OCT sensor and a structured light camera for automated large-field scanning. Adapted from [20].

For example, Finke et al. used an OCT system integrated into a motorized microscope with the goal of imaging the resection cavity in procedures such as glioblastoma resection to ensure that there are no residual tumor cells [99]. The authors developed custom algorithms for automatic positioning of the imaging system followed by 3D stitching of the resulting scans to obtain a large area field of view. Similarly, He et al. used a custom OCT system attached to a 6-DOF robotic arm to generate a large field of view, high resolution OCT angiogram of the whole mouse brain [98]. As robotic OCT systems become more common outside the intraoperative space, we anticipate more studies analyzing the data acquired by these systems.

3.2.3. Application for ophthalmic imaging

OCT has already been proven to be an excellent diagnostic tool in fields like ophthalmology where high-resolution volumetric imaging of micron-scale features is required. By integrating OCT into a robotic system, there is potential to expand access to this technology to populations that are unable to use traditional tabletop systems. Patients such as infants, children, and injured people may not be able to use a chinrest to prevent head movement during the OCT imaging session. To overcome these challenges, Draelos et al. proposed a robotically aligned OCT (RAOCT) system by attaching the OCT scanner to a 6-DOF robot arm end effector with RGB-D cameras and pupil cameras for motion estimation and object tracking [37,47]. This technology has the promise of improving access to eye care to areas without an available specialist physician and to patients unable to participate in tabletop systems. By moving the robot end effector, it can increase OCT imaging FOV through montaging [100] and compensate patient's head movement and even eyeball movement without a chinrest. Further work by Draelos et al. demonstrated the ability of this system to image individuals in multiple head orientations, as would be necessary with unconscious or bedbound patients [95]. The robotically-aligned OCT has been used to

Biomedical Optics EXPRESS

image a large cohort of patients in a remote clinical setting distanced from the provider, which would open the door for fully remote teleoperation [102]. There has also been work showing that these systems can image in non-specialist settings such as the emergency room and that those images can be used to triage eye conditions [103]. One recent study used robotically aligned OCT images to classify emergency room patients for referral to ophthalmology with high accuracy [104].

In other ophthalmology applications, research studies have focused on the combination of advanced robotic algorithms deployed on robot-mounted systems for efficient object scanning. Some research works have also been conducted to explore the use of precise lateral and axial positioning of robotically aligned OCT to image directionally reflective surfaces or perform angiography in the retina [105–107]. Fang et al. developed a robotically aligned system that can be used to image non-planar surfaces such as the anterior segment of the eye, offering a method to visualize the aqueous humor outflow pathway and Schlemm's canal to support glaucoma diagnostics [9]. Ahronovich et al. recently developed a handheld OCT system attached to a mechanical arm with 5 degrees-of-freedom control to compensate for hand tremor and subject motion when imaging pediatric retinas [94].

3.3. Roboticized OCT tools

Roboticized OCT tools are general OCT sensing systems integrated into instruments that augment surgical maneuvers. These tools frequently exhibit highly compact and customized design to meet application requirements. For example, in vitreoretinal and endoscopic surgery, conventional galvanometer-based OCT sensors cannot fit in the limited available space. Re-designing the OCT end-effector sensor suite is thus required, and novel optical designs have been proposed to tackle these geometric constraints [23]. We review research dedicated to OCT-guided robotic systems for micro-surgery and restricted environments, and group such systems into those where OCT sensing is primarily used for surgeon augmentation or robot feedback.

3.3.1. Surgeon-controlled tools

Microsurgical procedures require high dexterity and precision from surgeons. Even experienced and highly trained surgeons are susceptible to issues such as hand tremor. This motivated the development of advanced OCT sensor tools integrated with reliable robot control systems for safe surgical guidance. Previous research by the Kang group had proposed a handheld needle based system that utilized a piezoelectric linear motor driven by processed A-scans from a common-path swept-source OCT (CP-SSOCT) at the needle tip to compensate hand tremor for depth targeting on a bovine retina [108–110]. To account for the temporal delay between measurement and motor compensation, a Kalman filter was applied as a predictor to the position data. More recently, the group improved the design by using a real-time convolutional neural network to segment retinal boundaries before applying the Kalman filter [111]. Additionally, a linearly actuated CP-SSOCT probe has been developed to obtain angle measurements and perform tool depth correction for oblique injections [112]. This system, however, used two separate fiber outputs on either side of the needle at different heights along the shaft of the needle. Obtaining two distance measurements from separate fibers allowed for the oblique angle to be measured, which is useful information for subretinal injection applications. Koo et al. proposed a micro-surgical system to demonstrate the axial tremor compensation of two tools simultaneously during bimanual tasks [113]. In this study, surgical scissor blades and forceps were affixed with ball-lens CP-SSOCT fiber to directly measure tool height and compensated tremor with a piezoelectric linear motor. Furthermore, Yuan et al. developed an OCT micro-needle system to enable the integrated functions of therapy and diagnosis and demonstrated the feasibility by the *in vivo* mouse brain [24]. This work has reported an *in vivo* resolution of 1.7 μm axial and 5.7 μm transverse for fast volumetric imaging and demonstrated the feasibility of using OCT alongside with the laser scalpel for efficient cancer

Biomedical Optics EXPRESS

visualization and tissue removal. While most of these robot-OCT designs address axial tremor by utilizing a linear motor that controlled axial tremor, which is important in micro-surgical applications, they do not handle other degrees of freedom within surgeon movement.

3.3.2. Robot-controlled tools

Integrating the OCT fiber with a more dexterous robot can improve the tracking and compensation of surgeon movements (Fig. 4). This requires the miniaturization of complex robot systems and the computing power to process and potentially respond to larger amounts of OCT data. In early work, Balicki et al. integrated a common path OCT system into a microsurgical pick instrument to perform A-mode imaging for depth perception [117]. The experiments carried out with this device demonstrated the potential for the enforcement of safety barriers, distance tracking, and target tracking. This OCT system was coupled with a remote center of motion (RCM) to perform surgeon-in-the-loop co-manipulation functions. Additionally, Yang et al. demonstrated the coupling of a 6-DOF parallel robot for OCT image capture [115]. They designed a 6-DOF handheld micromanipulator instrument robot based off the Stewart-Gough configuration that performed active tremor compensation by tracking the probe's position and orientation with frequency-domain-multiplexed position-sensitive diodes [114,115,118]. This 6-DOF micromanipulator was then equipped with a common-path spectral domain OCT system and demonstrated automated volume capture using a spiral and pseudo-raster scan [115]. Yu et al. also utilized a Stewart-Gough based robot for micro-surgical instrument manipulation [116] and used it to demonstrate teleoperation of a 6-DOF Stewart-Gough based robot-OCT system that had a 7th-DOF to actuate the surgical forceps [58]. The OCT fiber was placed in between the graspers of the forceps and the OCT fiber was actuated within the probe tip to sweep and create B-scans for visualization. A surgeon manipulated a 7-DOF parallel robot that translated scaled surgeon movements to the instrument, where the 7th-DOF would open and close the forceps. The large DOF design allowed for a constraint on the RCM to prohibit unwanted tool translation at a pivot point as is preferred in sclerotomies [119]. Schoovaerts et al. proposed a novel design of a rotational OCT probe with an encoded fiber and distal half-ball lens [120]. This system has been targeted for intra-cochlear imaging in a tiny scanning space, and a system calibration method was proposed to capture the surface point cloud within the small cochlear structures. Similarly, Wang et al. added a common path OCT A-mode system to their autonomous robotic system designed to perform laparoscopic intestinal anastomosis [121]. Here, the OCT was used in conjunction with a machine learning network to detect missed or incorrect stitches in the anastomosis in real time. By transitioning handheld tools to robotically controlled ones, surgical actions can be performed without complex tremor. The speed and resolution of OCT are important considerations to design the robot controllers, and additional care must be taken into calibrating between the two systems and any parallel robots that may be used for tele-operation.

3.4. Robot endoscopic OCT

Endoscopic techniques have become more complex and mechanically demanding for endoscopists and surgeons. Therefore, there has been ample research and investment in robotic endoscopic systems that improve tool manipulation and stability [122] (Fig. 5). Many groups have found success in developing endoscopic OCT systems to offer a label-free alternative to existing endoscopic methods [16]. More recently, there has been research into streamlining this process by roboticizing the endoscope to allow for both manual and automated control with multiple degrees of freedom. Flexible robotic OCT endoscopes have been developed to allow for greater freedom of movement and control when using OCT to scan tissue in minimally invasive surgery or endoscopy [123,124]. These devices give the operating physician more opportunities to adjust their scanning path and utilize OCT image feedback without having to manually shift or remove the catheter or endoscope.

Biomedical Optics EXPRESS

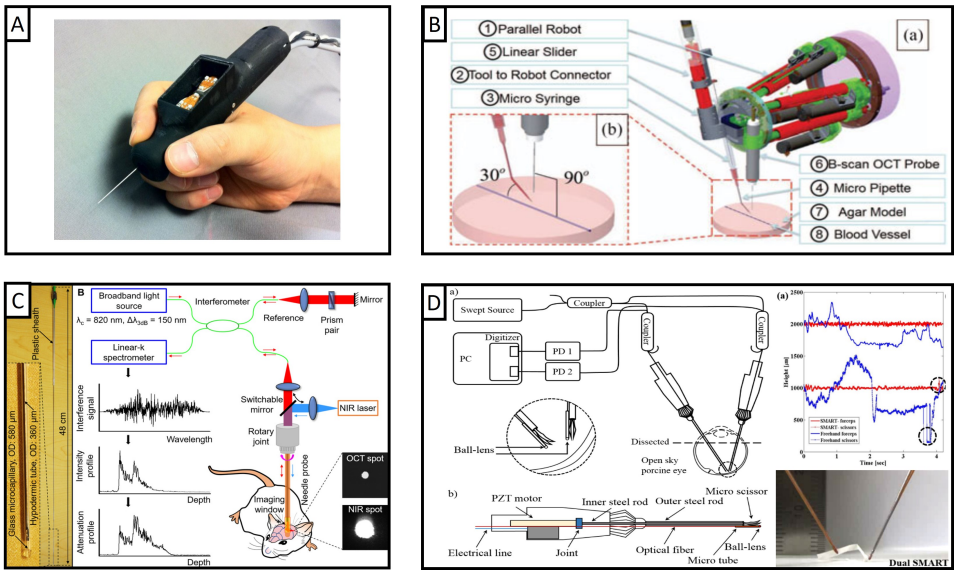

Fig. 4. Roboticized OCT sensing tools and associated robotic systems. (A) A handheld 6-DOF micromanipulator with an integrated OCT scanner [114,115]. Adapted from [115]. (B) A Stewart-Gough robot-OCT platform for precise oblique injection. Adapted from [116]. (C) An 800 nm OCT microneedle for ultrahigh-resolution deep-brain imaging and laser ablation. Adapted from [24]. (D) Linearly actuated bi-manual surgical tools with OCT guided depth correction. Adapted from [113].

3.4.1. Endoscope sensing and control

Robot endoscopic OCT offers expanded scanning capability in constrained environments, but poses challenges in the design of compact OCT optics systems and development of reliable guidance algorithms. For endoscope motion, Del Giudice et al. has developed an OCT-guided visual servoing framework for a continuum robot by using the volumetric OCT data [71]. This group developed an experimental approach to kinematic modeling as it directly determined the micro-motion Jacobian. Points from the OCT images gathered from the probe were selected to guide a needle fed through the endoscope into phantom tissue with closed-loop OCT visual servoing. Additionally, Zhang et al. developed a visual servoing control framework to obtain automatic scanning of a robotic endoscope with an OCT probe [15]. This proposed robotic endoscope was equipped with a monocular endoscopic camera and an OCT probe to perform automated tracking and object detection tasks. Endoscope movement was controlled by using an optimization based visual control strategy. The desired path of the endoscope is user-defined on the endoscopic image plane, and the authors solved a quadratic programming problem to drive automated movement to the desired position. In addition, endoscopic OCT designs have been incorporated with different robot control mechanisms and systems to target unique medical applications. For example, Yuan et al. proposed a telerobotic-OCT endoscope that uses rotatable diametrically magnetized cylinder permanent magnet to manipulate the endoscopic OCT probe for high-resolution imaging in complex lumens [17]. In summary, the innovations of endoscopic sensing and control methods have enabled the development of advanced system designs and robot control algorithms for target tissue diagnosis and imaging.

Biomedical Optics EXPRESS

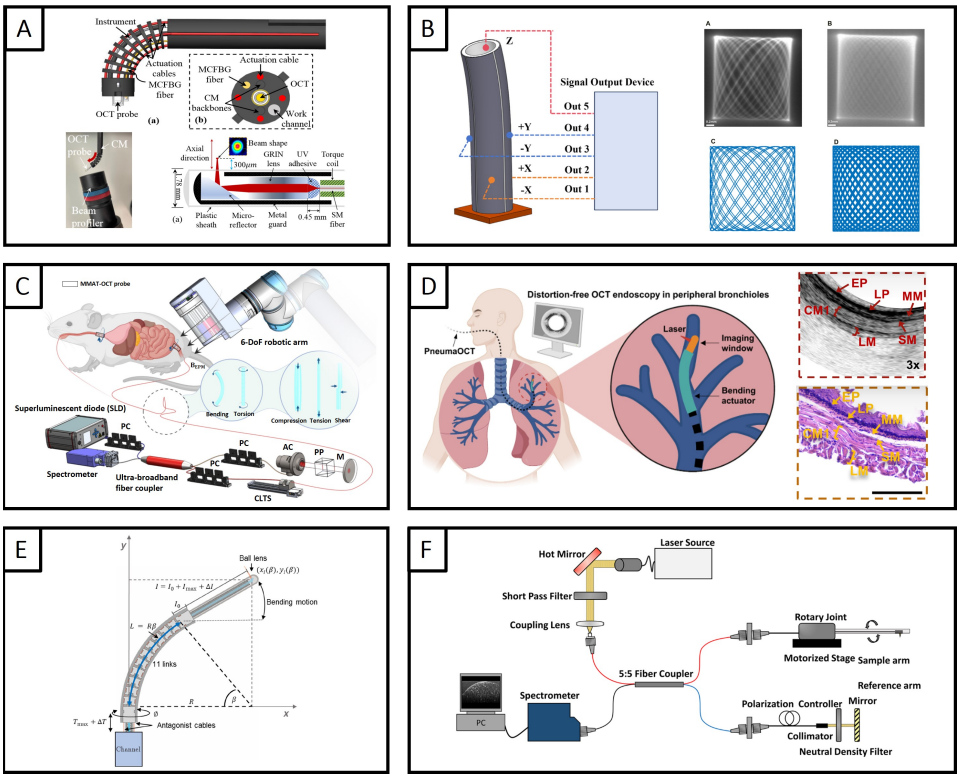

Fig. 5. Endoscopic robotic-OCT systems and scanners. (A) The distal end of an OCT neuroendoscope continuum robot. Adapted from [125]. (B) An endoscopic probe controlled by a quartered piezoelectric tube and Lissajous scans generated from sinusoidal voltage control. Adapted from [54]. (C) A motor-free telerobotic OCT endoscope for high-resolution intraluminal imaging (Figure and annotation size adapted from [17]). (D) A pneumatic OCT endoscope for tortuous and narrow internal lumens. Adapted from [26]. (E) The distal end of a robot steerable OCT-guided catheter. Adapted from [126]. (F) System design of endoscopic OCT system and high resolution imaging of a bioresorbable vascular scaffold implanted in swine coronary artery. Adapted from [25].

3.4.2. Multi-modality OCT endoscopes

OCT integrated into endoscopes can also support other imaging modalities or provide guidance for therapy. To guide the probe movement and surface scanning for malignant tissue detection in real time with probe confocal laser endomicroscopy (pCLE), Xu et al. developed an OCT-guided visual servoing endoscope to obtain and register clear pCLE images [127]. OCT images provided the depth information necessary to automatically maintain the proper probe distance to obtain sharp pCLE data as the probe moved forward. OCT can also be combined with laser scalpel techniques for endoscopic diagnosis and surgery [128]. For example, the Joos group coupled an OCT probe to a real-time laser ablation device that could potentially be enhanced with robotic capabilities [129]. This work demonstrated the feasibility of using real-time B-scan OCT imaging feedback for laser incisions during surgery. The advancement of both robotics and OCT over recent years has led to many opportunities to apply coupled systems to increasingly difficult biomedical tasks.

Biomedical Optics EXPRESS

3.4.3. Minimally-invasive endoscopic surgery

Robotic OCT endoscopes provide a means to deliver imaging systems and instruments to surgical sites through minimally-invasive means, especially in ophthalmology and neurosurgery. Ourak et al. proposed a unified system that combines an OCT A-scan fiber and a fiber Bragg grating (FBG) force sensor to perform retinal vein cannulation with a needle for *in vivo* animal studies [67]. Hu et al. proposed a novel design for obtaining intraocular endoscopic OCT scans of retina by using a piezoelectric tube to drive Lissajous scanning at the end of the fiber [54]. The tube was comprised of a hollow piezoelectric cylinder, where the OCT fiber was inserted, and the electrodes on the outer layer could be driven with equal but inverted voltages to cause it to bend in the direction of the electrodes.

In the interest of performing lesion assessments in the brain, Yan et al. developed a flexible OCT robotic neuroendoscope [125]. This cable-driven continuum manipulator included four actuation cables, the OCT fiber, a work channel for the insertion of surgical instruments, and a multi-core fiber Bragg grating for shape sensing. Xu et al. proposed a novel development of a patient-mounted neuro OCT system and demonstrated the feasibility with tumor imaging in a brain phantom as well as a mouse brain model [130]. This system incorporated a novel design of high-resolution OCT neuroendoscope and a patient-mounted skull-mounted robot into a unified system for minimally invasive neuroimaging.

3.4.4. Endoscopic diagnosis and intervention

OCT has developed a role for advanced sensing in gastroenterology, pulmonology, and cardiology where endoscopic and catheter-based interventions are already commonplace. Although not all of these approaches employ robotics to the degree of other integration strategies, we include them here for completeness as closely related technologies. An automatic scanning OCT catheter was developed by Caravaca et al. with the intention of improving imaging performance for gastroenterology applications [126]. The optical fiber was routed through the catheter and exited through a ball lens. For automatic scanning, the endoscope followed a pre-planned trajectory and proved more accurate and better spaced than manual scanning. Moreover, an endoscopic micro-OCT system was developed to image healthy and scaffolded swine coronary arteries with high resolution [25]. The spectral domain OCT output fiber was outfitted with a gradient-index (GRIN) lens and binary phase spatial filter to help improve resolution and depth-of-field. The fiber was fed into a laboratory-built optical rotary joint for 360 degrees of scanning and a motorized stage was used to feed the fiber forward. Zhang et al. introduced pneumatic OCT endoscopy to perform flexible scanning for internal luminal organs within the complex environment [26]. With a compact form factor with 2.8 mm diameter, this system combines a steerable catheter to achieve a bending angle of up to 237° for surgical navigation within a bronchial phantom.

4. Enabling technologies for robotic OCT systems

While conventional OCT imaging has demonstrated powerful synergies with robotic systems, there are several specific branches of OCT image augmentation which are specially relevant to OCT robotic guidance. In this section, we detail such augmentation and motivate them as features of importance in an OCT-guided robotic system.

4.1. Scan optimization

As a point-scanned modality, OCT is bound by fundamental trade-offs among resolution, field of view, and frame rate that can hinder its practical use in certain applications. For example, in real-time guidance applications such as ophthalmic surgery, there is simultaneous demand for high resolution, low latency, and high frame rate. Based on current surgical microscope standards, steep requirements are placed on all fronts, with resolutions on the order of 10s

Biomedical Optics EXPRESS

of microns, < 100 ms latency, 60 Hz display rate, and a field of view of several millimeters [131,132]. These demanding criteria make it difficult to optimize the overall OCT scanning speed. The development of efficient scanning algorithms can help overcome some of these limitations inherent in OCT imaging. As a depth-resolved modality, OCT requires another order of measurements at each lateral position that quickly make data bandwidths unmanageable when scaling to meet surgical microscope performance requirements. This motivates efficient scan pattern generation not only in the form of time-optimal fixed paths [133], but also in leveraging the positioning capabilities of galvanometer scanning mirrors. In addition, these methods can enable online adaptation of the scan pattern for more efficient use of limited bandwidths [134] and demonstrate potential in other applications requiring dense sampling of small objects that are distributed throughout a larger field [135]. This can be applied to resolve small surgical targets such as 100 μm subretinal injection needles with high resolution and frame rate.

For unique medical applications such as minimally invasive surgery or retinal imaging, the full field of view of the OCT scanner is not always required [136]. A smaller and more focused view can provide sufficient information for surgical guidance in certain circumstances. Therefore, improvement in OCT visualization becomes a joint optimization related to real-time OCT data processing and fast volumetric rendering [137,138], galvanometer scanning performance [139,140], and importance-based partial scene sampling [134]. By modeling galvanometer scanners as 2-DOF robots, existing robotics algorithms can provide novel insights into solving scan optimization problems.

Furthermore, a key problem with robotic OCT systems is the large volume of high-fidelity and detailed imaging data capture during scanning and real-time applications [43,141]. Onboard storage can quickly reach capacity, especially during long-duration robot scanning at high resolutions. Common solutions for efficient data management include data compression or image downsampling [62], selective data recording, and the development of efficient robot scanning algorithms to minimize unnecessary data recording. Other options include adjustments of OCT scan patterns to minimize the number of A-scans per B-scan image when detailed information about the image is not necessary. However, collection of a large volume of data storage can be inevitable in biomedical applications for detailed measurements of tissue structures, and thus data storage becomes a joint optimization with the robot planning algorithm, the total scan time of images, and the data compression strategy.

4.2. Refraction correction

Correction of image distortion due to light refraction is critical for ensuring physically accurate image data for use in the guidance of robotic systems. Without OCT light refraction and path length distortion correction, it is difficult to measure important geometries in scenes imaged through refractive structures, such as the cornea or even air-water interfaces [75]. In these cases, surgical tool or target localization is non-trivial, and distortion-correction techniques are required. For example, Westphal et al. proposed a 2D OCT light refraction correction algorithm based on Fermat's principle [142]. They reconstructed light distortion free OCT B-scans on the human eye's anterior chamber. Zhao et al. extended the 2D OCT light refraction correction to 3D through ray tracing [143]. They compared OCT refraction corrected corneal anterior and posterior curvatures with topography and a Scheimpflug camera. Ortiz et al. proposed a similar 3D OCT light refraction correction and also verified it through comparing corneal curvatures with Scheimpflug imaging [144]. Additionally, Tian et al. extended 3D OCT light refraction correction to corneal surgeries, in which the cornea is deformed due to tool tissue interaction, and quantitatively evaluated refraction correction residual errors [145]. These solutions to light refraction and correction challenges in OCT sensors play important roles in medical robotics to guarantee the correctness of sensor-to-tool system calibration and tissue deformation predictions.

Biomedical Optics EXPRESS

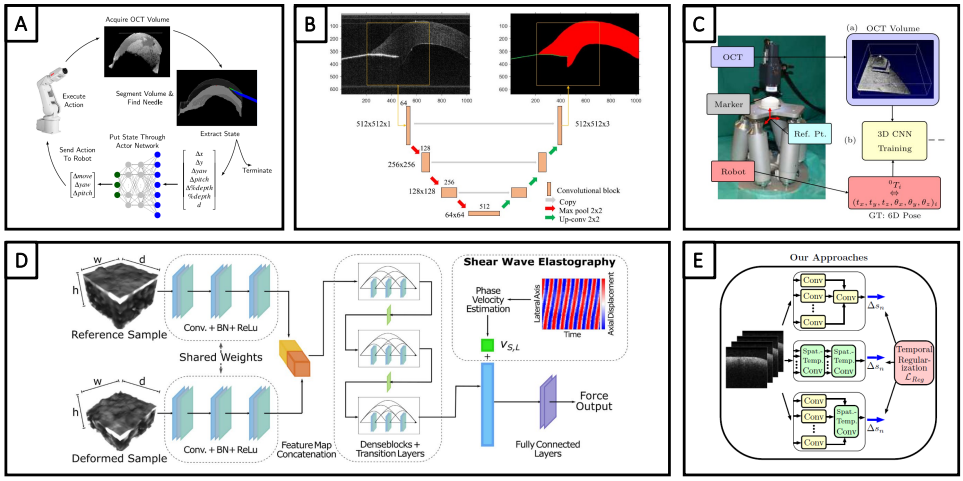

Fig. 6. Machine learning models for fundamental robotics problems with robotic OCT systems. (A) The flow diagram of the reinforcement learning framework for robotic needle insertion system (*ex vivo* human cornea target). Adapted from [56]. (B) An example of the OCT B-scan image segmentation by using the U-net deep learning architecture. Adapted from [65]. (C) A hexapod robot for pose estimation using deep learning models and volumetric OCT data. Adapted from [146]. (D) A multi-input deep learning framework for force estimation by using the shear wave elastography and volumetric OCT data. Adapted from [63]. (E) OCT image motion estimation with a deep learning architecture adjusted from the convolutional neural network modules via the temporal OCT volumes. Adapted from [60].

4.3. *Machine learning*

Robotic OCT systems must solve complex computer vision and motion planning problems that are well-suited for machine learning approaches (Fig. 6). A prevalent application for machine learning in robotic OCT platforms is surgical instrument localization. Deep learning image processing models have been readily applied to robotic sub-retinal injection systems to localize the needle tip and orientation, and were developed for use with OCT B-scan and volume data [51,65,77,78]. Additionally, deep learning has shown suitability for learning complex patterns from the large-size OCT volumetric data. Gessert et al. used a hexapod robot to generate a ground-truth dataset of OCT volumes of miniature fiducial markers in numerous orientations. These OCT volumes were used to train a deep learning model to predict marker orientation from the OCT volume [146]. Moreover, deep learning models have also been applied for 4D OCT data. Bengs et al. proposed a convolutional neural network (CNN) based model architecture to estimate the motion of a tissue model using spatial-temporal OCT data [60]. Unique network architectures, such as the combinations of multilayer perceptron (MLP) and CNN models, have also been incorporated into the tissue sensing system for abdominal tissue detection in automated suturing procedures [121]. The CNN model has also been used in the rupture detection of needle placement under soft-tissue deformation [147], where A-scan data is post-processed to formulate the complex OCT data configuration represented as images for deep learning models. For segmentation and classification of critical structures in OCT B-scan images, Shin et al. proposed a CNN-based segmentation method for lens fragments and demonstrated it in pig eye models [148]. Wang et al. have recently used OCT to automatically classify tissues to verify the quality of automated intestinal suturing [121]. Force estimation has been shown to be possible using OCT imaging through simulation-trained neural networks [149]. Another valuable use of machine

Biomedical Optics EXPRESS

learning for robotic OCT is the design of control schemes using learning from demonstration and reinforcement learning [150,151]. For example, Keller et al. applied these techniques to teach an OCT-guided robot how to perform a precise corneal needle insertion procedure [56]. These techniques can help train the robotic system to perform complex tasks without explicit programming of each step and an ability to improve over time. In summary, adaptations of deep learning models for B-scan and C-scan data have become the main trend in solving conventional OCT perception problems including segmentation, registration, and classification, as well as the robot control and planning problems. This can show greater generalization capability with large-scale medical datasets for medical applications.

5. Future directions

Despite extensive works that combine robotics and OCT to date, there are many opportunities to expand the intersection of these fields. We outline several avenues of future work in this section.

5.1. New hardware integrations

All robot-mounted OCT systems we review here are based on robot arms, which are serial manipulators with single kinematic chains (Fig. 3). Unless themselves mounted on mobile platforms, these systems have rigidly fixed bases, which restricts their operating environments and opportunities for deployment beyond the research lab. These devices therefore effectively function as static instruments to which specimens are brought for investigation. There is, therefore, an opportunity to consider other mounting strategies, such as developing robotic OCT systems based on drones, wheeled, legged, or humanoid robots. These mobile robotic platforms would enable the deployment of OCT in additional environments and increase the flexibility of large area OCT scanning. For example, a humanoid robotic OCT system could generalize large-area scanning to a full skin exam in dermatology settings. Such integrations would also bring the imaging capabilities of OCT to the point of care (e.g., ophthalmic) or point of application (e.g., storage device inspection), expanding access and versatility. With the recent accelerated development in soft robotics, researchers are also looking for solutions that integrate small sensors in soft robot systems for biomedical applications [152], where OCT can provide benefits over conventional sensor solutions in constrained and tiny environments (e.g., endoscopic OCT). Whether the OCT system should be integrated into the robot or a tool used temporarily by the robot is an important consideration, however, as robots become more general purpose.

Notably, many robotic OCT systems to-date employ a conventional point-scanning scheme, which necessitates scanning a single spot across the sample to assemble a full image or volume. From a practical standpoint, this often results from the design decision to separate the mass of the OCT scanner at the end-effector from the OCT engine (including the source, reference arm, interferometer, and detector) near the robot base while utilizing an optical fiber to connect the two. When this paradigm is used for real-time feedback and control, the time required to refresh the volume imposes limits on the system update rate. Parallel detection schemes, such as full-field OCT, provide an opportunity to avoid these limits [29,153]. Realizing this capability would likely require moving the entire OCT system to the robot end-effector or using free-space optical relay systems that are customized to the robot's kinematics. Both of these strategies would likely add considerable bulk and complexity to the robotic system in their current forms but would enable an update rate limited only by the detection/digitization scheme.

5.2. Image space alignment

Integrated robotics and OCT systems invariably require an accurate mapping between the robotic kinematic space and the OCT imaging space. System developers face two main challenges in this domain: calibration and refraction correction (Section 4.2). Calibration is commonly accomplished with a custom procedure that relies upon specialized fixtures/rigs and is unique to

Biomedical Optics EXPRESS

the individual combined robot and the OCT system. The creation of a new robotic OCT platform thus requires the design, implementation, and validation of a new calibration procedure, which may add considerable complexity to the system. Researchers in robotics and OCT would benefit from a collection of standard techniques and well-tested algorithms that would simplify the development of new integrated robotic and OCT systems. For example, the OpenCV library [154] and its optimized algorithms streamline the calibration of 2D cameras. A similar well-designed and rigorously-tested library for OCT systems would accelerate research progress. Such a library would require support for varying and application-specific scan patterns, anisotropic image resolution, and image distortions introduced by scanner optics.

The overwhelming majority of surgical or procedural robotic OCT assumes or requires a homogeneous index of refraction at the site of tool tissue interaction. As systems become more advanced and target areas with greater tissue complexity or operate beneath the tissue surface, index changes within the surgical scene will refract OCT light. These index changes are encoded within the OCT image and warp image derived data processed for the robot's perception system affecting the ability to generate accurate real-world coordinates for motion planning within tissue. Although many works have already addressed this issue (Section 4.2), these algorithms are computationally intensive and easily become the rate-limiting step for a real-time OCT perception system. Research in this area would benefit from real-time algorithms to produce geometrically-accurate surgical scene reconstructions not only for robotic guidance but also for real-time visualization. Opportunities exist for leveraging parallel computation devices (e.g., graphics processing units), sometimes equipped with dedicated ray tracing hardware, to achieve this reconstruction on demand.

5.3. *Interdisciplinary collaboration*

The robotics community, especially those working in medical technology development or clinical applications, would benefit from increased collaboration with the OCT community. Whereas cameras are a well-understood and characterized means for providing image feedback for robots, OCT is less well understood by the robotics community. However, the benefit of OCT over the better understood camera technologies is the ability to provide micrometer scale cross-sectional information within optically accessible tissues. In the context of surgery, we can consider this to be a better matching of the precision of a robot with a 3D vision system at the same scale. As an example, consider a thin surface pathology on top of normal tissue. A human hand may not have the precision or dexterity needed to accomplish the surgical task without damaging adjacent tissue, and a camera-based vision system would not have the depth resolution and contrast needed to visually distinguish thin pathology from underlying normal tissue. Robotics enables the precision needed to remove only that thin surface pathology without disturbing the underlying normal tissue, and OCT provides the cross-sectional vision needed to see and distinguish the thin surface layer from the underlying normal tissue. Additional examples include laser ablations where precise amounts of tissue are removed: robotics helps the laser access the tissue with precision while OCT has the depth resolution needed to monitor the tissue change as it is ablated by the laser.

6. Conclusion

Robotic OCT is a fast-growing field addressing important challenges and necessitating the interdisciplinary collaborations between researchers in robotics, optics, biomedical engineering, and medicine. These challenges center around the integration of the strength of OCT for visualization and the capabilities of robotics for manipulation to create systems that increase the utility of both for biomedical applications. OCT brings an optical sensor capable of near real-time, micro-scale cross-sectional visualizations, and robotics brings the capability for controlled micro-scale movements in multiple axes. In this article, we reviewed different strategies that have been

Biomedical Optics EXPRESS

reported for performing this integration — robot-adjacent OCT, robot-mounted OCT, roboticized OCT tools, and robot endoscopic OCT — and their applications for large area scanning, medical diagnostics, surgical visualization and guidance, surgical end-effector assistance, and endoscopy. Machine learning also plays a role in the integration of OCT and robotics with the ability to analyze the sensed image content and create motion plans based on the image information and goals of the action. Research thus far has demonstrated the feasibility and potential of robotic OCT, and continued development and growth in this field are expected to impact biomedical applications, particularly in medicine, ranging from automated robot-based OCT diagnostics to robot-assisted procedural interventions utilizing OCT feedback.

Funding. National Institutes of Health (R00 EY034200, R21 EY033959, R01 EY035534, F31 EY035168); National Science Foundation (NRT 2125528); Research to Prevent Blindness (Physician-Scientist Award); University of Michigan.

Acknowledgments. The authors dedicate this work to the memory of Joseph A. Izatt, an outstanding mentor to many, a pioneer in OCT and robotics, and founding editor-in-chief of *Biomedical Optics Express*.

Contributions. GM and MD planned and organized the review. GM contributed introduction, background and robot-mounted OCT systems. MM contributed probe-based robotic OCT systems, including endoscopic OCT. YT contributed ophthalmic robotic OCT and OCT-based tissue modeling and automated surgery. AN contributed translational applications of robotic OCT. HS contributed machine learning applications in robotic OCT. RT contributed robotics for OCT field of view expansion. GM, MM, YT, AN, HS, RT, RPM, ANK, and MD revised the manuscript. RPM, ANK, and MD supervised the project.

Disclosures. MD: Duke University (P), Horizon Surgical (C). ANK: Leica Microsystems (P, R), Johnson & Johnson Vision (F). RPM: Leica Microsystems (P, R), Johnson & Johnson Vision (F).

Data availability. This review paper presents no original data. The authors refer requests for data to the authors of the reviewed work in question.

References

1. D. Huang, E. A. Swanson, C. P. Lins, *et al.*, "Optical coherence tomography," Science **254**(5035), 1178–1181 (1991).
2. C. K. Hitzenberger, "Optical coherence tomography," Opt. Express **26**(18), 24240–24259 (2018).
3. J. A. Izatt, M. R. Hee, E. A. Swanson, *et al.*, "Micrometer-scale resolution imaging of the anterior eye in vivo with optical coherence tomography," Arch. Ophthalmol. **112**(12), 1584–1589 (1994).
4. M. R. Hee, J. A. Izatt, E. A. Swanson, *et al.*, "Optical coherence tomography of the human retina," Arch. Ophthalmol. **113**(3), 325–332 (1995).
5. A. R. Ran, C. C. Tham, P. P. Chan, *et al.*, "Deep learning in glaucoma with optical coherence tomography: a review," Eye **35**(1), 188–201 (2021).
6. R. T. Yanagihara, C. S. Lee, D. S. W. Ting, *et al.*, "Methodological challenges of deep learning in optical coherence tomography for retinal diseases: a review," Trans. Vis. Sci. Tech. **9**(2), 11 (2020).
7. N. Eladawi, M. Elmogy, M. Ghazal, *et al.*, "Classification of retinal diseases based on OCT images," Front. Biosci. **23**(1), 247–264 (2018).
8. Y. Wang, S. Liu, S. Lou, *et al.*, "Application of optical coherence tomography in clinical diagnosis," J. X-Ray Sci. Technol. **27**, 995–1006 (2019).
9. R. Fang, P. Zhang, T. Zhang, *et al.*, "Imaging the conventional outflow pathway with robotic visible-light optical coherence tomography," in *Optical Coherence Tomography and Coherence Domain Optical Methods in Biomedicine XXVIII*, vol. PC12830 R. A. Leitgeb and Y. Yasuno, eds., International Society for Optics and Photonics (SPIE, 2024), p. PC128302D.
10. X. Ma, M. Moradi, X. Ma, *et al.*, "Large area kidney imaging for pre-transplant evaluation using real-time robotic optical coherence tomography," Commun. Eng. **3**(1), 122 (2024).
11. H. Pan, C. W. Lim, K. King, *et al.*, "Active motion cancellation for robotic optical coherence tomography of moving eyes: A nystagmus phantom study," in *2024 International Symposium on Medical Robotics (ISMR)*, (IEEE, 2024), pp. 1–7.
12. S. Guo, N. Sarfaraz, W. Gensheimer, *et al.*, "Optical coherence tomography guided robotic device for autonomous needle insertion in cornea transplant surgery," in *2019 IEEE/RSJ International Conference on Intelligent Robots and Systems (IROS)*, (2019), pp. 7068–7074.
13. J. D. Opfermann, M. Barbic, M. Khrenov, *et al.*, "A novel wax based piezo actuator for autonomous deep anterior lamellar keratoplasty (piezo-dalk)," in *2021 IEEE/RSJ International Conference on Intelligent Robots and Systems (IROS)*, (2021), pp. 757–764.
14. M. Draelos, G. Tang, B. Keller, *et al.*, "Optical coherence tomography guided robotic needle insertion for deep anterior lamellar keratoplasty," IEEE Trans. Biomed. Eng. **67**, 2073–2083 (2020).
15. Z. Zhang, B. Rosa, O. Caravaca-Mora, *et al.*, "Image-guided control of an endoscopic robot for OCT path scanning," IEEE Robot. Autom. Lett. **6**(3), 5881–5888 (2021).

Biomedical Optics EXPRESS

16. M. J. Gora, M. J. Suter, G. J. Tearney, *et al.*, "Endoscopic optical coherence tomography: technologies and clinical applications," Biomed. Opt. Express **8**(5), 2405–2444 (2017).
17. S. Yuan, C. Xu, B. Cui, *et al.*, "Motor-free telerobotic endomicroscopy for steerable and programmable imaging in complex curved and localized areas," Nat. Commun. **15**(1), 7680 (2024).
18. K. W. Nam, J. Park, I. Y. Kim, *et al.*, "Application of stereo-imaging technology to medical field," Healthc. Inform Res. **18**(3), 158–163 (2012).
19. L. Ma and B. Fei, "Comprehensive review of surgical microscopes: technology development and medical applications," J. Biomed. Opt. **26**(01), 010901 (2021).
20. X. Li, Y. Huang, and Q. Hao, "Automated robot-assisted wide-field optical coherence tomography using structured light camera," Biomed. Opt. Express **14**(8), 4310–4325 (2023).
21. N. Hungr, I. Bricault, P. Cinquin, *et al.*, "Design and validation of a CT-and MRI-guided robot for percutaneous needle procedures," IEEE Trans. Robot. **32**(4), 973–987 (2016).
22. J. Wang, Y. Xu, and S. A. Boppart, "Review of optical coherence tomography in oncology," J. Biomed. Opt. **22**(12), 1–121711 (2017).
23. O. M. Carrasco-Zevallos, C. Viehland, B. Keller, *et al.*, "Review of intraoperative optical coherence tomography: technology and applications," Biomed. Opt. Express **8**(3), 1607–1637 (2017).
24. W. Yuan, D. Chen, R. Sarabia-Estrada, *et al.*, "Theranostic OCT microneedle for fast ultrahigh-resolution deep-brain imaging and efficient laser ablation in vivo," Sci. Adv. **6**(15), eaaz9664 (2020).
25. J. Kim, S. Kim, J. W. Song, *et al.*, "Flexible endoscopic micro-optical coherence tomography for three-dimensional imaging of the arterial microstructure," Sci. Rep. **10**(1), 9248 (2020).
26. T. Zhang, S. Yuan, C. Xu, *et al.*, "Pneumaoct: Pneumatic optical coherence tomography endoscopy for targeted distortion-free imaging in tortuous and narrow internal lumens," Sci. Adv. **10**(35), eadp3145 (2024).
27. R. Leitgeb, F. Placzek, E. Rank, *et al.*, "Enhanced medical diagnosis for doctors: a perspective of optical coherence tomography," J. Biomed. Opt. **26**(10), 100601 (2021).
28. J. M. Schmitt, "Optical coherence tomography (OCT): a review," IEEE J. Sel. Top. Quantum Electron. **5**(4), 1205–1215 (1999).
29. R. A. Leitgeb, "En face optical coherence tomography: a technology review [invited]," Biomed. Opt. Express **10**(5), 2177–2201 (2019).
30. M. Pircher and R. J. Zawadzki, "Review of adaptive optics OCT (AO-OCT): principles and applications for retinal imaging," Biomed. Opt. Express **8**(5), 2536–2562 (2017).
31. W. Drexler and J. G. Fujimoto, *Optical Coherence Tomography: Technology and Applications* (Springer Science & Business Media, 2008).
32. J. A. Izatt and M. A. Choma, "Theory of optical coherence tomography," in *Optical Coherence Tomography: Technology and Applications*, (Springer, 2008), pp. 47–72.
33. Z. Yaqoob, J. Wu, and C. Yang, "Spectral domain optical coherence tomography: a better OCT imaging strategy," BioTechniques **39**(sup6), S6–S13 (2005).
34. J. Fujimoto and E. Swanson, "The development, commercialization, and impact of optical coherence tomography," Invest. Ophthalmol. Vis. Sci. **57**(9), OCT1–OCT13 (2016).
35. B. He, Y. Zhang, L. Zhao, *et al.*, "Robotic-OCT guided inspection and microsurgery of monolithic storage devices," Nat. Commun. **14**(1), 5701 (2023).
36. S. Song, J. Xu, and R. K. Wang, "Long-range and wide field of view optical coherence tomography for in vivo 3D imaging of large volume object based on akinetic programmable swept source," Biomed. Opt. Express **7**(11), 4734–4748 (2016).
37. M. Draelos, P. Ortiz, R. Qian, *et al.*, "Contactless optical coherence tomography of the eyes of freestanding individuals with a robotic scanner," Nat. Biomed. Eng. **5**(7), 726–736 (2021).
38. Y. Huang, X. Li, J. Liu, *et al.*, "Robotic-arm-assisted flexible large field-of-view optical coherence tomography," Biomed. Opt. Express **12**(7), 4596–4609 (2021).
39. F. Rüfer, A. Schröder, and C. Erb, "White-to-white corneal diameter: normal values in healthy humans obtained with the orbscan ii topography system," Cornea **24**(3), 259–261 (2005).
40. T. Lifshitz, J. Levy, S. Rosen, *et al.*, "Central corneal thickness and its relationship to the patient's origin," Eye **20**(4), 460–465 (2006).
41. J. Pulido, C. Pulido, S. Bakri, *et al.*, "The use of 31-gauge needles and syringes for intraocular injections," Eye **21**(6), 829–830 (2007).
42. M. Zhou, H. Roodaki, A. Eslami, *et al.*, "Needle segmentation in volumetric optical coherence tomography images for ophthalmic microsurgery," Appl. Sci. **7**(8), 748 (2017).
43. S. Lotz, M. Göb, S. Böttger, *et al.*, "Large area robotically assisted optical coherence tomography (lara-oct)," Biomed. Opt. Express **15**(6), 3993–4009 (2024).
44. P. E. Dupont, B. J. Nelson, M. Goldfarb, *et al.*, "A decade retrospective of medical robotics research from 2010 to 2020," Sci. Robot. **6**(60), eabi8017 (2021).
45. R. H. Taylor, A. Menciassi, G. Fichtinger, *et al.*, "Medical robotics and computer-integrated surgery," Springer handbook of robotics **9**, 1657–1684 (2016).
46. S. E. Salcudean, H. Moradi, D. G. Black, *et al.*, "Robot-assisted medical imaging: A review," Proc. IEEE **110**(7), 951–967 (2022).

Biomedical Optics EXPRESS

47. M. Draelos, P. Ortiz, R. Qian, *et al.*, "Automatic optical coherence tomography imaging of stationary and moving eyes with a robotically-aligned scanner," in *2019 International Conference on Robotics and Automation (ICRA)*, (IEEE, 2019), pp. 8897–8903.
48. J. Sprenger, T. Saathoff, and A. Schlaefer, "Automated robotic surface scanning with optical coherence tomography," in *2021 IEEE 18th International Symposium on Biomedical Imaging (ISBI)*, (IEEE, 2021), pp. 1137–1140.
49. R. R. Perez, J. Jivraj, and V. X. D. Y. M.d, "Intraoperative optical coherence tomography of the cerebral cortex using a 7 degree-of freedom robotic arm," in *Clinical and Translational Neurophotonics*, vol. 10050 (SPIE, 2017), pp. 81–86.
50. Y. Tian, M. Draelos, G. Tang, *et al.*, "Toward autonomous robotic micro-suturing using optical coherence tomography calibration and path planning," in *2020 IEEE International Conference on Robotics and Automation (ICRA)*, (2020), pp. 5516–5522.
51. K. Mach, S. Wei, J. W. Kim, *et al.*, "OCT-guided robotic subretinal needle injections: A deep learning-based registration approach," in *2022 IEEE International Conference on Bioinformatics and Biomedicine (BIBM)*, (IEEE, 2022), pp. 781–786.
52. P. Zhang, J. W. Kim, P. Gehlbach, *et al.*, "Autonomous needle navigation in subretinal injections via ioct," IEEE Robot. Autom. Lett. **9**(5), 4154–4161 (2024).
53. A. Ebrahimi, M. G. Urias, N. Patel, *et al.*, "Adaptive control improves sclera force safety in robot-assisted eye surgery: A clinical study," IEEE Trans. Biomed. Eng. **68**(11), 3356–3365 (2021).
54. J. Hu, S. Wu, G. Shi, *et al.*, "Design of an endoscopic OCT probe based on piezoelectric tube with quartered outside electrodes," Front. Bioeng. Biotechnol. **12**, 1391630 (2024).
55. N. Gessert, J. Beringhoff, C. Otte, *et al.*, "Force estimation from OCT volumes using 3D CNNs," Int J CARS **13**(7), 1073–1082 (2018).
56. B. Keller, M. Draelos, K. Zhou, *et al.*, "Optical coherence tomography-guided robotic ophthalmic microsurgery via reinforcement learning from demonstration," IEEE Transactions on Robotics **36**(4), 1207–1218 (2020).
57. J. Jivraj, C. Chen, D. Barrows, *et al.*, "Optical coherence tomography for dynamic axial correction of an optical end-effector for robot-guided surgical laser ablation," Opt. Eng. **58**(05), 1–054106 (2019).
58. H. Yu, J.-H. Shen, R. J. Shah, *et al.*, "Evaluation of microsurgical tasks with OCT-guided and/or robot-assisted ophthalmic forceps," Biomed. Opt. Express **6**(2), 457–472 (2015).
59. J. T. Wilson, M. J. Gerber, S. W. Prince, *et al.*, "Intraocular robotic interventional surgical system (IRISS): Mechanical design, evaluation, and master-slave manipulation," The International Journal of Medical Robotics and Computer Assisted Surgery **14**, e1842 (2018).
60. M. Bengs, N. Gessert, M. Schlüter, *et al.*, "Spatio-temporal deep learning methods for motion estimation using 4D OCT image data," Int. J. CARS **15**(6), 943–952 (2020).
61. S. Pannek, S. Dehghani, M. Sommersperger, *et al.*, "Exploring the needle tip interaction force with retinal tissue deformation in vitreoretinal surgery," in *2024 IEEE International Conference on Robotics and Automation (ICRA)*, (IEEE, 2024), pp. 16999–17005.
62. N. Gessert, M. Bengs, M. Schlüter, *et al.*, "Deep learning with 4D spatio-temporal data representations for OCT-based force estimation," Med. Image Anal. **64**, 101730 (2020).
63. M. Neidhardt, R. Mieling, M. Bengs, *et al.*, "Optical force estimation for interactions between tool and soft tissues," Sci. Rep. **13**(1), 506 (2023).
64. M. Zhu, W. Chang, L. Jing, *et al.*, "Dual-modality optical diagnosis for precise in vivo identification of tumors in neurosurgery," Theranostics **9**(10), 2827–2842 (2019).
65. I. Park, H. K. Kim, W. K. Chung, *et al.*, "Deep learning based real-time OCT image segmentation and correction for robotic needle insertion systems," IEEE Robot. Autom. Lett. **5**(3), 4517–4524 (2020).
66. W. Edwards, G. Tang, Y. Tian, *et al.*, "Data-driven modelling and control for robot needle insertion in deep anterior lamellar keratoplasty," IEEE Robot. Autom. Lett. **7**(2), 1526–1533 (2022).
67. M. Ourak, J. Smits, L. Esteveny, *et al.*, "Combined OCT distance and FBG force sensing cannulation needle for retinal vein cannulation: in vivo animal validation," Int. J. CARS **14**(2), 301–309 (2019).
68. J. Smits, M. Ourak, A. Gijbels, *et al.*, "Development and experimental validation of a combined FBG force and OCT distance sensing needle for robot-assisted retinal vein cannulation," in *2018 IEEE international conference on robotics and automation (ICRA)*, (IEEE, 2018), pp. 129–134.
69. M. J. Gerber, J.-P. Hubschman, and T.-C. Tsao, "Automated retinal vein cannulation on silicone phantoms using optical-coherence-tomography-guided robotic manipulations," IEEE/ASME Transactions on Mechatronics **26**(5), 2758–2769 (2020).
70. S. Dehghani, M. Sommersperger, P. Zhang, *et al.*, "Robotic navigation autonomy for subretinal injection via intelligent real-time virtual ioct volume slicing," in *2023 IEEE International Conference on Robotics and Automation (ICRA)*, (IEEE, 2023), pp. 4724–4731.
71. G. Del Giudice, A. L. Orekhov, J.-H. Shen, *et al.*, "Investigation of micromotion kinematics of continuum robots for volumetric OCT and OCT-guided visual servoing," IEEE/ASME Trans. Mechatron. **26**(5), 2604–2615 (2020).
72. Y. Baran, K. Rabenorosoa, G. J. Laurent, *et al.*, "Preliminary results on oct-based position control of a concentric tube robot," in *2017 IEEE/RSJ International Conference on Intelligent Robots and Systems (IROS)*, (IEEE, 2017), pp. 3000–3005.

Biomedical Optics EXPRESS

73. M. Ourak, B. Tamadazte, and N. Andreff, "Partitioned camera-OCT based 6 DoF visual servoing for automatic repetitive optical biopsies," in *2016 IEEE/RSJ International Conference on Intelligent Robots and Systems (IROS)*, (IEEE, 2016), pp. 2337–2342.
74. C.-W. Chen, Y.-H. Lee, M. J. Gerber, *et al.*, "Intraocular robotic interventional surgical system (IRISS): semi-automated OCT-guided cataract removal," The International Journal of Medical Robotics and Computer Assisted Surgery **14**, e1949 (2018).
75. B. Keller, M. Draelos, G. Tang, *et al.*, "Real-time corneal segmentation and 3D needle tracking in intrasurgical OCT," Biomed. Opt. Express **9**(6), 2716–2732 (2018).
76. J. Weiss, N. Rieke, M. A. Nasseri, *et al.*, "Fast 5d of needle tracking in IOCT," International Journal of Computer Assisted Radiology and Surgery **13**(6), 787–796 (2018).
77. M. Zhou, X. Guo, M. Grimm, *et al.*, "Needle detection and localisation for robot-assisted subretinal injection using deep learning," in *CAAI Transactions on Intelligence Technology* (2023).
78. M. Zhou, X. Wang, J. Weiss, *et al.*, "Needle localization for robot-assisted subretinal injection based on deep learning," in *2019 International Conference on Robotics and Automation (ICRA)*, (2019), pp. 8727–8732. ISSN: 2577-087X.
79. P. Xu, M. Ourak, G. Borghesan, *et al.*, "Fast OCT based needle tracking for retinal microsurgery using dynamic spiral scanning," IEEE Trans. Med. Robot. Bionics **6**(4), 1502–1511 (2024).
80. M. Sommersperger, J. Weiss, M. Ali Nasseri, *et al.*, "Real-time tool to layer distance estimation for robotic subretinal injection using intraoperative 4D OCT," Biomed. Opt. Express **12**(2), 1085–1104 (2021).
81. N. Wang, X. Zhang, D. Stoyanov, *et al.*, "Vision-and-force-based compliance control for a posterior segment ophthalmic surgical robot," IEEE Robot. Autom. Lett. **8**(11), 6875–6882 (2023).
82. H. G. Shin, I. Park, K. Kim, *et al.*, "Corneal suturing robot capable of producing sutures with desired shape for corneal transplantation surgery," IEEE Transactions on Robotics **37**(1), 304–312 (2021).
83. M. Draelos, B. Keller, G. Tang, *et al.*, "Real-time image-guided cooperative robotic assist device for deep anterior lamellar keratoplasty," in *2018 IEEE international conference on robotics and automation (ICRA)*, (IEEE, 2018), pp. 4013–4018.
84. M. Zhou, M. Hamad, J. Weiss, *et al.*, "Towards robotic eye surgery: Marker-free, online hand-eye calibration using optical coherence tomography images," IEEE Robot. Autom. Lett. **3**(4), 3944–3951 (2018).
85. M. Zhou, X. Hao, A. Eslami, *et al.*, "6dof needle pose estimation for robot-assisted vitreoretinal surgery," IEEE Access **7**, 63113–63122 (2019).
86. S. L. Charreyron, Q. Boehler, A. N. Danun, *et al.*, "A magnetically navigated microcannula for subretinal injections," IEEE Trans. Biomed. Eng. **68**(1), 119–129 (2021).
87. T. Edwards, K. Xue, H. Meenink, *et al.*, "First-in-human study of the safety and viability of intraocular robotic surgery," Nat. Biomed. Eng. **2**(9), 649–656 (2018).
88. M. T. El-Haddad and Y. K. Tao, "Advances in intraoperative optical coherence tomography for surgical guidance," Curr. Opin. Biomed. Eng. **3**, 37–48 (2017).
89. M. Draelos, B. Keller, C. Toth, *et al.*, "Teleoperating robots from arbitrary viewpoints in surgical contexts," in *2017 IEEE/RSJ International Conference on Intelligent Robots and Systems (IROS)*, (IEEE, 2017), pp. 2549–2555.
90. M. Draelos, B. Keller, C. Viehland, *et al.*, "Real-time visualization and interaction with static and live optical coherence tomography volumes in immersive virtual reality," Biomed. Opt. Express **9**(6), 2825–2843 (2018).
91. N. Tang, J. Fan, P. Wang, *et al.*, "Microscope integrated optical coherence tomography system combined with augmented reality," Opt. Express **29**(6), 9407–9418 (2021).
92. J. Sprenger, T. Saathoff, and A. Schlaefer, "Automated robotic surface scanning with optical coherence tomography," in *2021 IEEE 18th International Symposium on Biomedical Imaging (ISBI)*, (2021), pp. 1137–1140. ISSN: 1945–8452.
93. C. Wu, X. Li, Y. Huang, *et al.*, "System calibration and pose optimization for robotic-arm-assisted optical coherence tomography," in *2021 International Conference on Optical Instruments and Technology: Optical Systems, Optoelectronic Instruments, Novel Display, and Imaging Technology*, vol. 12277 (SPIE, 2022), pp. 147–153.
94. E. Ahronovich, J.-H. Shen, T. J. Vadakkan, *et al.*, "Five degrees-of-freedom mechanical arm with remote center of motion (rcm) device for volumetric optical coherence tomography (oct) retinal imaging," Biomed. Opt. Express **15**(2), 1150–1162 (2024).
95. M. Draelos, P. Ortiz, A. Narawane, *et al.*, "Robotic optical coherence tomography of human subjects with posture-invariant head and eye alignment in six degrees of freedom," in *2023 International Symposium on Medical Robotics (ISMR)*, (IEEE, 2023), pp. 1–7.
96. P. Ortiz, M. Draelos, C. Viehland, *et al.*, "Robotically aligned optical coherence tomography with 5 degree of freedom eye tracking for subject motion and gaze compensation," Biomed. Opt. Express **12**(12), 7361–7376 (2021).
97. P. Ortiz, M. Draelos, R. P. McNabb, *et al.*, "Autoaligning and autofocusing robotic optical coherence tomography of the retina for subject motion, gaze, and defocus compensation," in *Optical Coherence Tomography and Coherence Domain Optical Methods in Biomedicine XXV*, vol. 11630 (SPIE, 2021), p. 116300H.
98. B. He, Y. Zhang, Z. Meng, *et al.*, "Whole brain micro-vascular imaging using robot assisted optical coherence tomography angiography," IEEE J. Sel. Top. Quantum Electron. **29**, 1–9 (2022).

Biomedical Optics EXPRESS

99. M. Finke, S. Kantelhardt, A. Schlaefer, *et al.*, "Automatic scanning of large tissue areas in neurosurgery using optical coherence tomography," The International Journal of Medical Robotics and Computer Assisted Surgery **8**, 327–336 (2012).
100. P. Ortiz, M. Draelos, A. Narawane, *et al.*, "Robotically-aligned optical coherence tomography with gaze tracking for live image montaging of the retina," in *2022 International Conference on Robotics and Automation (ICRA)*, (2022), pp. 3783–3789.
101. E. Sun, R. Fang, and H. F. Zhang, "Montaging multiple optical coherence tomography volumes," in *Optical Coherence Tomography and Coherence Domain Optical Methods in Biomedicine XXVIII*, vol. PC12830 (SPIE, 2024), p. PC128300P.
102. R. McNabb, P. Ortiz, K.-M. Roh, *et al.*, "Contactless, autonomous robotic alignment of optical coherence tomography for in vivo evaluation of diseased retinas," Research Square (2023).
103. A. Song, K.-M. Roh, J. B. Lusk, *et al.*, "Robotic optical coherence tomography retinal imaging for emergency department patients: A pilot study for emergency physicians' diagnostic performance," Annals of Emergency Medicine **81**(4), 501–508 (2023).
104. A. Song, J. B. Lusk, K.-M. Roh, *et al.*, "RobOCTNet: Robotics and Deep Learning for Referable Posterior Segment Pathology Detection in an Emergency Department Population," Trans. Vis. Sci. Tech. **13**(3), 12 (2024).
105. A. Narawane, P. Ortiz, M. Draelos, *et al.*, "Automated volumetric retinal imaging with complete visualization of henle's fiber layer using robotically aligned optical coherence tomography," *Ophthalmic Technologies XXXII*, (SPIE, 2022), p. PC119410R.
106. A. Narawane, M. Draelos, P. Ortiz, *et al.*, "Robotically-aligned optical coherence tomography angiography with multiple illumination angles for enhanced vessel visualization," in *Ophthalmic Technologies XXXIII*, (SPIE, 2023), p. PC123600J.
107. R. P. McNabb, Y. Tian, P. Ortiz, *et al.*, "In vivo ophthalmic robotically aligned optical coherence tomography with interchangeable cornea and retina imaging modules," in *Ophthalmic Technologies XXXIV*, (SPIE, 2024), p. PC1282412.
108. G. W. Cheon, Y. Huang, J. Cha, *et al.*, "Accurate real-time depth control for cp-ssoct distal sensor based handheld microsurgery tools," Biomed. Opt. Express **6**(5), 1942–1953 (2015).
109. C. Song, P. L. Gehlbach, and J. U. Kang, "Active tremor cancellation by a 'smart' handheld vitreoretinal microsurgical tool using swept source optical coherence tomography," Opt. Express **20**(21), 23414–23421 (2012).
110. J. U. Kang, J.-H. Han, X. Liu, *et al.*, "Common-path optical coherence tomography for biomedical imaging and sensing," J. Opt. Soc. Korea **14**(1), 1–13 (2010).
111. S. Lee and J. U. Kang, "CNN-based CP-OCT sensor integrated with a subretinal injector for retinal boundary tracking and injection guidance," J. Biomed. Opt. **26**(06), 068001 (2021).
112. J. Im and C. Song, "Oblique injection depth correction by a two parallel OCT sensor guided handheld smart injector," Biomed. Opt. Express **12**(2), 926–939 (2021).
113. D. Koo, H.-C. Park, P. L. Gehlbach, *et al.*, "Development and preliminary results of bimanual smart micro-surgical system using a ball-lens coupled OCT distance sensor," Biomed. Opt. Express **7**(11), 4816–4826 (2016).
114. S. Yang, R. A. MacLachlan, and C. N. Riviere, "Manipulator design and operation of a six-degree-of-freedom handheld tremor-canceling microsurgical instrument," IEEE/ASME Trans. Mechatron. **20**(2), 761–772 (2014).
115. S. Yang, M. Balicki, R. A. MacLachlan, *et al.*, "Optical coherence tomography scanning with a handheld vitreoretinal micromanipulator," in *2012 Annual International Conference of the IEEE Engineering in Medicine and Biology Society*, (IEEE, 2012), pp. 948–951.
116. H. Yu, J.-H. Shen, K. M. Joos, *et al.*, "Calibration and integration of b-mode optical coherence tomography for assistive control in robotic microsurgery," IEEE/ASME Trans. Mechatron. **21**(6), 2613–2623 (2016).
117. M. Balicki, J.-H. Han, I. Iordachita, *et al.*, "Single fiber optical coherence tomography microsurgical instruments for computer and robot-assisted retinal surgery," in *Medical Image Computing and Computer-Assisted Intervention–MICCAI 2009: 12th International Conference, London, UK, September 20-24, 2009*, Proceedings, Part I 12, (Springer, 2009), pp. 108–115.
118. R. A. MacLachlan and C. N. Riviere, "High-speed microscale optical tracking using digital frequency-domain multiplexing," IEEE Trans. Instrum. Meas. **58**(6), 1991–2001 (2009).
119. H. Yu, J.-H. Shen, K. M. Joos, *et al.*, "Design, calibration and preliminary testing of a robotic telemanipulator for OCT guided retinal surgery," in *2013 IEEE International Conference on Robotics and Automation*, (IEEE, 2013), pp. 225–231.
120. M. Schoovaerts, M. Ourak, G. Borghesan, *et al.*, "OCT-based intra-cochlear imaging and 3D reconstruction: ex vivo validation of a robotic platform," Int. J. CARS **19**(5), 917–927 (2024).
121. Y. Wang, S. Wei, R. Zuo, *et al.*, "Automatic and real-time tissue sensing for autonomous intestinal anastomosis using hybrid MLP-DC-CNN classifier-based optical coherence tomography," Biomed. Opt. Express **15**(4), 2543–2560 (2024).
122. T. A. d. C. Visconti, J. P. Otoch, and E. L. d. A. Artifon, "Robotic endoscopy. a review of the literature," Acta Cir. Bras. **35**(2), e202000206 (2020).
123. G. Del Giudice, L. Wang, J.-H. Shen, *et al.*, "Continuum robots for multi-scale motion: Micro-scale motion through equilibrium modulation," in *2017 IEEE/RSJ International Conference on Intelligent Robots and Systems (IROS)*, (2017), pp. 2537–2542.

Biomedical Optics EXPRESS

124. O. C. Mora, P. Zanne, L. Zorn, *et al.*, "Steerable oct catheter for real-time assistance during teleoperated endoscopic treatment of colorectal cancer," Biomed. Opt. Express **11**(3), 1231–1243 (2020).
125. J. Yan, P. Chen, J. Chen, *et al.*, "Design and evaluation of a flexible sensorized robotic OCT neuroendoscope," in *2023 International Symposium on Medical Robotics (ISMR)*, (IEEE, 2023), pp. 1–7.
126. O. Caravaca-Mora, P. Zanne, G. Liao, *et al.*, "Automatic intraluminal scanning with a steerable endoscopic optical coherence tomography catheter for gastroenterology applications," J. Optical Microsystems **3**(01), 011005 (2023).
127. X. Xu, R. Tang, and S. Zuo, "A novel OCT servoing control method for endomicroscopy surface scanning," Biomedical Signal Processing and Control **83**, 104719 (2023).
128. A. Gunalan and L. S. Mattos, "Towards oct-guided endoscopic laser surgery–a review," Diagnostics **13**(4), 677 (2023).
129. Z. Li, J. H. Shen, J. A. Kozub, *et al.*, "Miniature forward-imaging b-scan optical coherence tomography probe to guide real-time laser ablation," Lasers Surg. Med. **46**(3), 193–202 (2014).
130. C. Xu, Z. Fang, H. Gao, *et al.*, "Patient-mounted neuro optical coherence tomography for targeted minimally invasive micro-resolution volumetric imaging in brain in vivo," Advanced Intelligent Systems **2024** Early View, 2400488 (2024).
131. S. Rizzo, G. Abbruzzese, A. Savastano, *et al.*, "3D surgical viewing system in ophthalmology: Perceptions of the surgical team," Retina **38**(4), 857–861 (2018).
132. D. Ta Kim and D. Chow, "The effect of latency on surgical performance and usability in a three-dimensional heads-up display visualization system for vitreoretinal surgery," Graefe's Arch. Clin. Exp. Ophthalmol. **260**(2), 471–476 (2022).
133. M. Draelos, "Time-optimal spiral trajectories with closed-form solutions," IEEE Robot. Autom. Lett. **8**(4), 2213–2220 (2023).
134. M. Draelos, C. Viehland, R. P. McNabb, *et al.*, "Adaptive point-scan imaging beyond the frame rate–resolution limit with scene-reactive scan trajectories," Optica **9**(11), 1276–1288 (2022).
135. Y. Tian, M. Draelos, R. P. McNabb, *et al.*, "Efficient 3D cell tracking using adaptive scanning OCT," in *Optical Coherence Tomography and Coherence Domain Optical Methods in Biomedicine XXVII*, (SPIE, 2023), p. PC123670L.
136. A. Britten, P. Matten, J. Weiss, *et al.*, "Surgical microscope integrated mhz ss-oct with live volumetric visualization," Biomed. Opt. Express **14**(2), 846–865 (2023).
137. Y. Jian, K. Wong, and M. V. Sarunic, "Graphics processing unit accelerated optical coherence tomography processing at megahertz axial scan rate and high resolution video rate volumetric rendering," J. Biomed. Opt. **18**(02), 1–026002 (2013).
138. J. Probst, D. Hillmann, E. Lankenau, *et al.*, "Optical coherence tomography with online visualization of more than seven rendered volumes per second," J. Biomed. Opt. **15**(02), 1–026014 (2010).
139. V.-F. Duma, P. Tankam, J. Huang, *et al.*, "Optimization of galvanometer scanning for optical coherence tomography," Appl. Opt. **54**(17), 5495–5507 (2015).
140. V. Duma, "Command functions of open loop galvanometer scanners with optimized duty cycles," Theoretical and Applied Mechanics Letters **2**(4), 043005 (2012).
141. W. Draxinger, D. Theisen-Kunde, L. Schützeck, *et al.*, "High speed 4d in-vivo oct imaging of the human brain: creating high density datasets for machine learning toward identification of malign tissue in real time," in *High-Speed Biomedical Imaging and Spectroscopy VIII*, vol. 12390 (SPIE, 2023), pp. 43–48.
142. V. Westphal, A. M. Rollins, S. Radhakrishnan, *et al.*, "Correction of geometric and refractive image distortions in optical coherence tomography applying Fermat's principle," Opt. Express **10**(9), 397–404 (2002).
143. M. Zhao, A. N. Kuo, and J. A. Izatt, "3D refraction correction and extraction of clinical parameters from spectral domain optical coherence tomography of the cornea," Opt. Express **18**(9), 8923–8936 (2010).
144. S. Ortiz, D. Siedlecki, I. Grulkowski, *et al.*, "Optical distortion correction in optical coherence tomography for quantitative ocular anterior segment by three-dimensional imaging," Opt. Express **18**(3), 2782–2796 (2010).
145. Y. Tian, M. Draelos, R. P. McNabb, *et al.*, "Optical coherence tomography refraction and optical path length correction for image-guided corneal surgery," Biomed. Opt. Express **13**(9), 5035–5049 (2022).
146. N. Gessert, M. Schlüter, and A. Schlaefer, "A deep learning approach for pose estimation from volumetric OCT data," Med. Image Anal. **46**, 162–179 (2018).
147. S. Latus, J. Sprenger, M. Neidhardt, *et al.*, "Rupture detection during needle insertion using complex oct data and cnns," IEEE Trans. Biomed. Eng. **68**(10), 3059–3067 (2021).
148. C. Shin, M. J. Gerber, Y.-H. Lee, *et al.*, "Semi-automated extraction of lens fragments via a surgical robot using semantic segmentation of oct images with deep learning-experimental results in ex vivo animal model," IEEE Robot. Autom. Lett. **6**(3), 5261–5268 (2021).
149. A. Mendizabal, R. Sznitman, and S. Cotin, "Force classification during robotic interventions through simulation-trained neural networks," Int. J. CARS **14**(9), 1601–1610 (2019).
150. D. Zhang, W. Si, W. Fan, *et al.*, "From teleoperation to autonomous robot-assisted microsurgery: A survey," Mach. Intell. Res. **19**(4), 288–306 (2022).
151. T. Huang, K. Chen, B. Li, *et al.*, "Guided reinforcement learning with efficient exploration for task automation of surgical robot," in *2023 IEEE International Conference on Robotics and Automation (ICRA), (IEEE, 2023)*, pp. 4640–4647.

Biomedical Optics EXPRESS

152. Y. Qiu, A. Ashok, C. C. Nguyen, *et al.*, "Integrated sensors for soft medical robotics," Small **20**(22), 2308805 (2024).
153. O. Thouvenin, C. Apelian, A. Nahas, *et al.*, "Full-field optical coherence tomography as a diagnosis tool: Recent progress with multimodal imaging," Appl. Sci. **7**(3), 236 (2017).
154. G. Bradski, "The OpenCV Library," Dr. Dobb's Journal of Software Tools (2000).